Journal of Asian Earth Sciences 81 (2014) 38–52

Contents lists available at ScienceDirect

Journal of Asian Earth Sciences

journal homepage: www.elsevier.com/locate/jseaes

Crustal and upper mantle S-wave velocity structures across the Taiwan Strait from ambient seismic noise and teleseismic Rayleigh wave analyses

Yu-Chih Huang [a,b,*], Huajian Yao [c,d], Francis T. Wu [e], Wen-Tzong Liang [a], Bor-Shouh Huang [a], Cheng-Horng Lin [a,b], Kuo-Liang Wen [f,g]

[a] Institute of Earth Sciences, Academia Sinica, Taipei, Taiwan
[b] Taiwan Volcano Observatory – Tatun, Taipei, Taiwan
[c] Laboratory of Seismology and Physics of Earth's Interior, School of Earth and Space Sciences, University of Science and Technology of China, Hefei, China
[d] Mengcheng National Geophysical Observatory, University of Science and Technology of China, Hefei, China
[e] Department of Geological Sciences, State University of New York at Binghamton, Binghamton, NY, USA
[f] Department of Earth Sciences, National Central University, Taoyuan, Taiwan
[g] National Center for Research on Earthquake Engineering, Taipei, Taiwan

ARTICLE INFO

Article history:
Received 7 June 2013
Received in revised form 26 November 2013
Accepted 27 November 2013
Available online 7 December 2013

Keywords:
S-wave velocity structure
Crust and upper mantle
Taiwan Strait
Ambient seismic noise
Surface wave two-station method

ABSTRACT

Although orogeny tapers off in western Taiwan large and small earthquakes do occur in the Taiwan Strait, a region largely untouched in previous studies owing mostly to logistical reasons. But the overall crustal structure of this region is of particular interest as it may provide a hint of the proto-Taiwan before the orogeny.

By combining time domain empirical Green's function (TDEGF) from ambient seismic noise using station-pairs and traditional surface wave two-station method (TS) we are able to construct Rayleigh wave phase velocity dispersion curves between 5 and 120 s. Using Broadband Array in Taiwan for Seismology (BATS) stations in Taiwan and in and across the Strait we are able to derive average 1-D Vs structures in different parts of this region. The results show significant shear velocity differences in the upper 15 km crust as expected. In general, the highest Vs in the upper crust observed in the coastal area of Mainland China and the lowest Vs appears along the southwest offshore of the Taiwan Island; they differ by about 0.6–1.1 km/s. For different parts of the Strait, the upper crust Vs structures are lower in the middle by about 0.1–0.2 km/s relative to those in the northern and southern parts. The upper mantle Vs structure (Moho – 150 km) beneath the Taiwan Strait is about 0.1–0.3 km/s lower than the AK135 model. The overall crustal thickness is approximately 30 km, much thinner and less variable than under the Taiwan Island. The inversion of seismic velocity structures using shorter period band dispersion data in the sea areas with water depth deeper than 1000 m should take water layer into consideration except for the continental shelves.

1. Introduction

1.1. Regional environment

The Taiwan Strait between Mainland China and Taiwan sits on the Eurasian continental shelf, with an average water depth of less than 50 m, and has an area of around 200×300 km^2. Offshore southwestern Taiwan the water deepens to 1000 m (Fig. 1). Adjacent to the Taiwan Strait to the southwest is the South China Sea and to the east is the Taiwan orogeny. It is the result of collision between the Eurasian Plate and the Philippine Sea Plate, currently converging at a rate of 7–8 cm/yr in the direction of N307°E (e.g., Seno et al., 1993; Yu et al., 1997; Hsu et al., 2009; Seno and Kawanishi, 2009) (Fig. 1). Being close to plate boundaries, the Taiwan orogen, including the Foothills, is seismically very active (e.g., Wu, 1978; Rau and Wu, 1995; Wu et al., 1997, 2007; Kim et al., 2005) but the Strait is much less so in comparison. Without any major bathymetric relief, the Strait is assumed to be tectonically relatively inactive. However, significant intraplate earthquakes did occur in the Taiwan Strait. The locations and mechanisms for most seismic events were not well-determined due to a sparsity of stations. Only a few large recent earthquakes, such as the $M = 6.5$, 16 September 1994 earthquake (Kao and

* Corresponding author. Address: Institute of Earth Sciences, Academia Sinica, 128 Academia Road, Section 2, Nankang, Taipei 11529, Taiwan. Tel.: +886 2 2861-2283; fax: +886 2 2861 3582.
E-mail address: nativemanncu@gmail.com (Y.-C. Huang).

1367-9120/$ - see front matter © 2013 Elsevier Ltd. All rights reserved.
http://dx.doi.org/10.1016/j.jseaes.2013.11.023

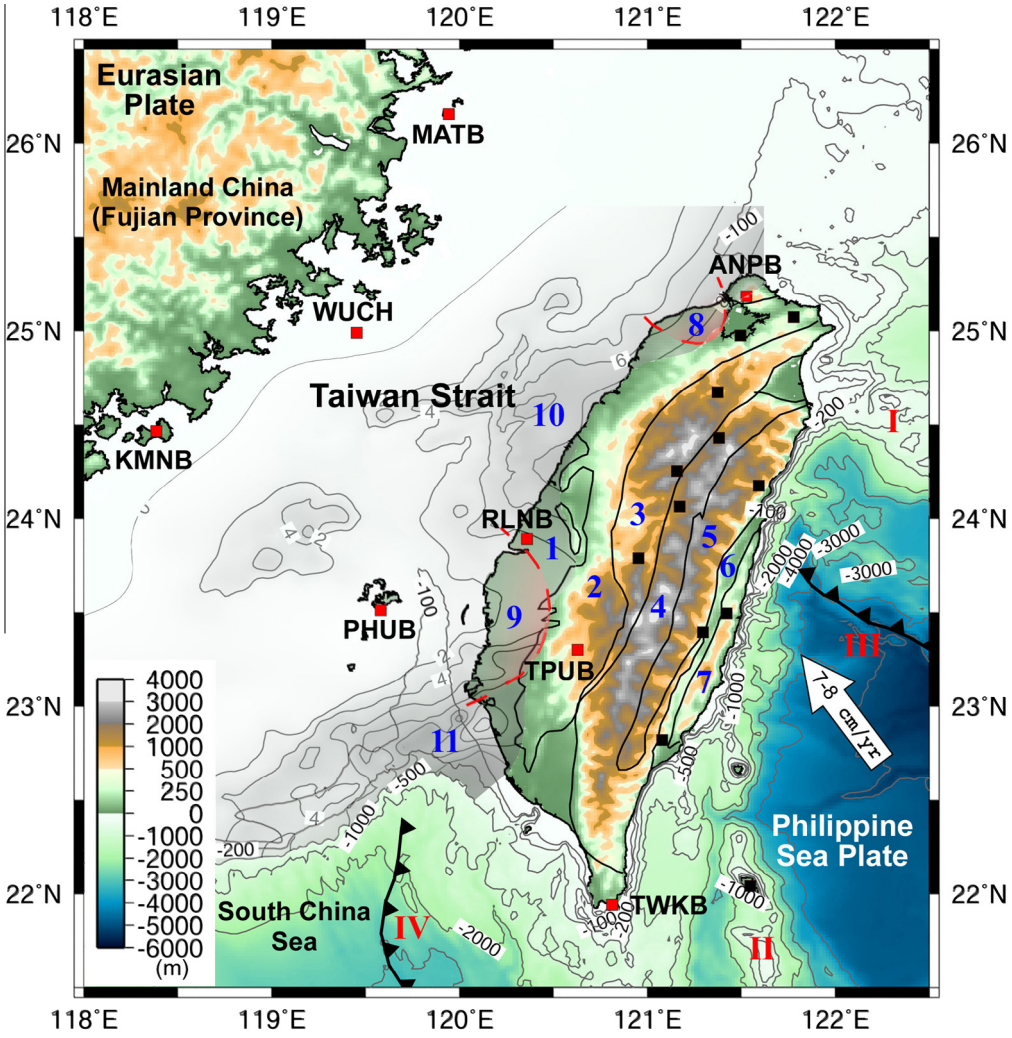

Fig. 1. Tectonic units, tectonic environment, topography, and bathymetry adjacent to the Taiwan Strait with BATS stations (black and red squares) operated by IESAS. The data of stations marked with red squares and names are analyzed in this study. Tectonic units on Taiwan Island are according to Ho (1988) and the convergent rate between the Eurasian Plate and Philippine Sea Plate is around 7–8 cm/yr. Cenozoic sedimentary foreland basins in the Taiwan Strait are from Lin et al. (2003). (For interpretation of the references to colour in this figure legend, the reader is referred to the web version of this article.)

Wu, 1996; Huang et al., 1999), have been studied albeit with limited station coverage. The 1604 $M \sim 8.0$ Quanzhou earthquake is the largest known historical tsunamigenic earthquake in the Taiwan Strait (Lee et al., 1976; Huang et al., 1999).

1.2. Previous studies in the Taiwan Strait

Over the past few decades, most of the tectonic research (e.g., Wu, 1978; Suppe, 1981; Angelier, 1986; Tsai, 1986; Ho, 1988; Teng, 1990; Hsu and Sibuet, 1995; Sibuet and Hsu, 1997; Wu et al., 1997; Lin, 2000, 2002) and velocity determination (e.g., Roecker et al., 1987; Rau and Wu, 1995; Ma et al., 1996; Chen et al., 2003; Kim et al., 2005; Wu et al., 2007; Wang et al., 2009) were focused on the Taiwan Island. Two comprehensive projects TAICRUST (Yeh et al., 1998; Shih et al., 1998; Nakamura et al., 1998; McIntosh et al., 2005) and TAIGER (TAiwan Integrated GEodynamics Research; http://taiger.binghamton.edu/index.htm; Kuo-Chen et al., 2012) were also more focused on the Taiwan Island and its eastern offshore region rather than the Taiwan Strait.

Relatively shallow crust mapping using marine multi-channel seismic reflection experiments had been conducted, mainly for resource exploration. Lin and Watts (2002) and Lin et al. (2003) compiled seismic reflection profiles and well data in western Taiwan and the Taiwan Strait to determine the Cenozoic stratigraphic and tectonic development of the foreland basin. Huang et al. (1998) found that the Pn velocity beneath the Taiwan Strait is 8.2 ± 0.2 km/s and higher than those beneath the Taiwan Island and Taiwan eastern offshore region. Some studies (e.g., Kao et al., 2003; Kim et al., 2004; Wang et al., 2010a, 2010b) employed the receiver function method to retrieve 1-D S-wave velocity (Vs)

structure and Moho discontinuity depths beneath BATS (Broadband Array in Taiwan for Seismology) stations. Although the exact Moho discontinuity depths beneath Taiwan Island varied with different studies, the two BATS stations KMNB and MATB (see locations in Fig. 1) on the southeastern coast of China showed robust results. The Moho depths are 28–32 km and 31–34 km beneath KMNB and MATB, respectively. Hsieh et al. (2010) constructed a Bouguer gravity anomaly map and estimated the average crustal thickness in the Taiwan Strait which is around 30 km and thinner than Taiwan Island and Fujian Province. Ai et al. (2007) and Huang et al. (2010b) tried to resolve velocity structures beneath southeastern China with Taiwan and Fujian data but they are targeted mostly on mantle transition zones. The recently comprehensive project ATSEE (Across Taiwan Strait Explosion Experiment) studied the crustal structures beneath the Taiwan area based on active explosion source experiments. Their preliminary crustal thickness across the Taiwan Strait is about 26 km (Wang et al., 2011).

1.3. Outline of this research

This research aims at the derivation of average 1-D Vs structures along a few two-station paths across the Taiwan Strait using data from several BATS stations (operated by the Institute of Earth Sciences, Academia Sinica; IESAS). A classic two-station (TS) surface wave dispersion study can be used to determine structures between the stations– if a teleseism occurs nearly along the same great circle. The modern time domain empirical Green's Functions (TDEGFs) from ambient seismic noise in the shorter period band 5–30 s can be determined between any two stations with continuous records. By combining the traditional surface wave two-station dispersions in the longer period band 10–120 s and those from the TDEGFs, we can invert for both the 1-D velocity structures for the crust and the uppermost mantle. Comparing the obtained 1-D Vs structures along different paths in the Taiwan Strait will provide some constraints for understanding more about the tectonic environment in the surrounding region.

2. Data

In late 1992, IESAS started to establish the BATS network (e.g., Kao et al., 1998; Liang et al., 2004; Wang et al., 2010a). For this study we selected 7 permanent BATS stations and one temporary station (WUCH) deployed by IESAS (red squares in Fig. 1) on both sides of the Taiwan Strait with a total of 28 station-pairs. Five of the selected permanent stations operated prior to 2000 till now, except that PHUB started from May 2002 and RLNB started from June 2004 (http://bats.earth.sinica.edu.tw/Station/BATS_Stn_Summary.html). Due to the shorter operation time of PHUB and RLNB than the other stations and a limited bandwidth for extracting dispersion data from ambient seismic noise, we hence selected the nearby TPUB station (55 km inland) as a supplementary station. The temporary WUCH station only operated from mid-2004 to mid-2006 and changed its name to VWUC as a permanent station with real-time satellite transmission after September 2009.

3. Ambient seismic noise cross-correlation analysis

It has been shown that the stable TDEGF of surface waves can be derived from the cross-correlation of continuous-recorded ambient seismic noise, which can be used to obtain subsurface shear wave velocity structures (e.g., Shapiro and Campillo, 2004; Sabra et al., 2005a, 2005b; Shapiro et al., 2005; Yao et al., 2006). This method does not require seismic signals from earthquakes or active sources but uses continuous ambient seismic noise. Furthermore, TDEGF has several advantages over other traditional seismic waveform analysis methods, including few restrictions on seismic sources distribution and study regions, more homogeneous lateral resolution than body wave tomography, and the ability to resolve velocity structure at shallower depths than earthquake-based surface wave tomography.

Over the past few years, ambient seismic noise tomography has been widely used to investigate crustal and upper mantle structures all over the world, including the United States (e.g., Shapiro et al., 2005; Bensen et al., 2008, 2009; Lin et al., 2008), China (e.g., Yao et al., 2006, 2008; Zheng et al., 2008; Li et al., 2009; Yang et al., 2010), Europe (e.g., Yang et al., 2007; Stehly et al., 2009; Li et al., 2010), South Korea (e.g., Kang and Shin, 2006; Cho et al., 2007), New Zealand (e.g., Lin et al., 2007), Africa (e.g., Yang et al., 2008a), Australia (e.g., Saygin and Kennett, 2010) and so forth. The dimensions of these studies mostly range from hundreds to thousands of kilometers and the average inter-station distances are about tens to hundreds of kilometers. The period ranges of surface wave dispersion curves from TDEGF are usually between 5 and 50 s. Up to now, there are also a few ambient seismic noise tomography studies in the Taiwan regions (e.g., Huang et al. (2010a); You et al., 2010; Huang et al., 2012).

The sources of ambient seismic noise mainly come from ocean microseisms (e.g., Stehly et al., 2006; Yang and Ritzwoller, 2008a; Yao et al., 2009); continental shelves are considered as dominant source regions of ambient seismic noise (e.g., Bromirski, 2001; Webb, 2007; Traer et al., 2008; Yang and Ritzwoller, 2008a). The Taiwan Strait is mainly a continental shelf and consequently a main source region for ambient seismic noise. In contrast to numerous applications of ambient seismic noise studies for continents, only a few studies investigate oceanic structure using ambient seismic noise (e.g., Lin et al., 2006; Harmon et al., 2007; Yao et al., 2011). Lin et al. (2006) confirmed that ambient seismic noise has been observed to propagate coherently along oceanic paths between continent stations. Harmon et al. (2007) and Yao et al. (2011) successfully used the ambient seismic noise recorded at ocean bottom seismometers to recover both the fundamental mode and the first higher mode Rayleigh wave for studying the crust and uppermost mantle structure near the Eastern Pacific Rise. Therefore, it is possible to obtain the 1-D Vs structures of oceanic paths across the Taiwan Strait using ambient seismic noise.

Here we use 7 years of continuously-recorded data of ambient seismic noise of LHZ channel (1 Hz sampling rate of the vertical component) from 2000 to 2006 for the permanent stations in Fig. 1 (see Section 2 for the detail). The operation time of the temporary WUCH station was 2 years from mid-2004 to mid-2006. Seismic Analysis Code (SAC) 2000 (Goldstein et al., 2003; http://www.iris.edu/manuals/sac/manual.html) was used for baseline correction (removing the mean and the trend) of raw data and data selection. After removing the instrument response, we applied one-bit cross-correlation (e.g., Larose et al., 2004; Shapiro and Campillo, 2004) to monthly recordings in the period band 5–50 s to enhance the signal to noise ratio (SNR) of TDEGFs. Yao et al. (2009) showed that TDEGFs from one-bit cross-correlation are nearly identical with or without earthquake signals in the period band 10–20 s. Other methods like clipping large seismic event signals directly (e.g., Sabra et al., 2005b; Marzorati and Bindi, 2008) or spectrum whitening of waveforms (e.g., Cho et al., 2007; Yang et al., 2007) also can enhance the SNR and obtain stable TDEGFs. Cupillard and Capdeville (2010) showed the consistency of TDEGFs from the methods mentioned above using synthetic waveforms.

After one-bit cross-correlation, the monthly TDEGF in the period band 5–50 s for each station-pair was obtained. Fig. 2 shows the

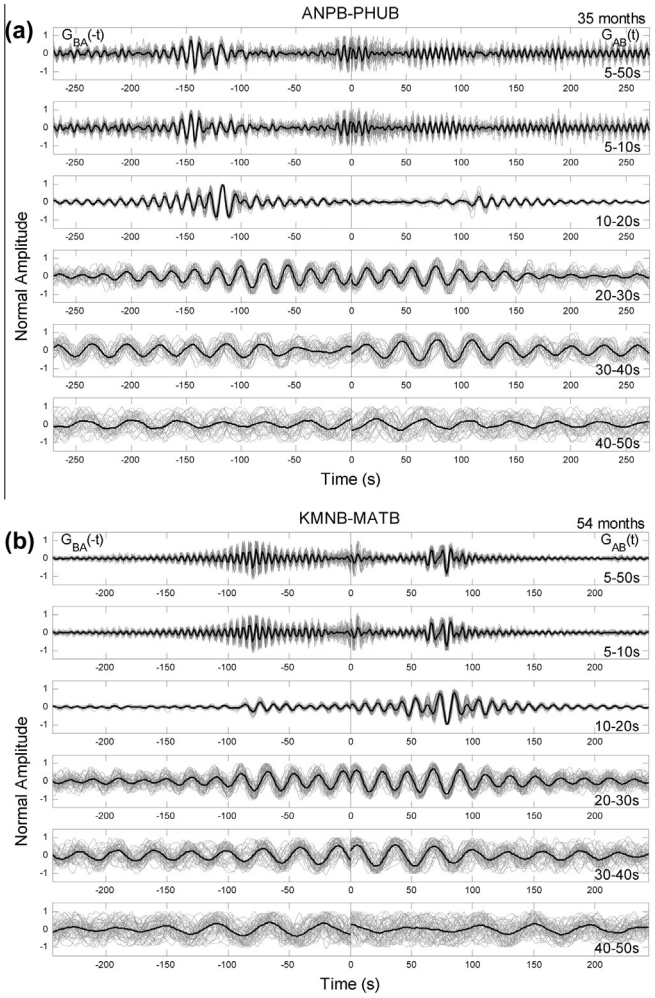

Fig. 2. TDEGFs of two station-pairs (a) ANPB-PHUB and (b) KMNB-MATB on both sides of the Taiwan Strait. TDEGFs are band-pass filtered in six period bands: 5–50 s, 5–10 s, 10–20 s, 20–30 s, 30–40 s, and 40–50 s. Gray lines show TDEGFs from monthly data and black lines show the stacked TDEGFs of all monthly TDEGFs. The upper-right corner also shows the number of months for data analysis.

TDEGFs in the period band 5–50 s and other five narrower period bands of the two station-pairs ANPB-PHUB and KMNB-MATB on either side of the Taiwan Strait. Since the 5–50 s broad band TDEGFs are very similar to 5–10 s period band TDEGFs, this implies that the dominant ambient seismic noise is in the 5–10 s period band, i.e., the secondary microseism band. The TDEGFs are more stable at the two ocean microseism period bands (5–10 s and 10–20 s). Although the inter-station distances of these two station-pairs are similar (Fig. 1), the propagation time of surface waves in TDEGFs is different. The propagation time between ANPB and PHUB is about 150 s in the 5–10 s period band and 120 s in the 10–20 s period band (Fig. 2a). Conversely, the propagation time between KMNB and MATB is about 80 s in both the 5–10 s and 10–20 s period bands (Fig. 2b), which is much faster than between ANPB and PHUB. This implies a high average Vs structure in the upper and perhaps also middle crust beneath KMNB-MATB than beneath ANPB-PHUB.

Fig. 3 shows TDEGFs of the other two station-pairs, KMNB-WUCH and MATB-WUCH. Although WUCH is a temporary station with shorter data duration, the monthly TDEGFs are quite stable in the 5–10 s and 10–20 s period bands. The stability of the monthly TDEGFs deteriorates in the longer period bands (e.g., 30–40 s and 40–50 s) (Figs. 2 and 3). Meanwhile, WUCH is located nearly at the middle of KMNB and MATB (Fig. 1). The propagation time between KMNB-WUCH and MATB-WUCH is also roughly half of that between KMNB-MATB. Fig. 4 shows stacked TDEGFs of all station-pairs at 10–20 s and 20–30 s period bands. The main surface wave signals (maximum amplitudes) have an apparent propagation wavespeed between 2–3.5 km/s in the 10–20 s period band and 3–4 km/s in the 20–30 s period band. In Section 5, we measured Rayleigh wave phase velocity dispersion only in the period band 5–30 s for each station-pair from the stacked TDEGF using the phase-velocity image analysis technique by Yao et al. (2006).

4. Earthquake surface wave two-station analysis

The surface wave two-station (TS) method is usually applied to study crust and upper mantle structures at a regional scale (e.g., Polet and Kanamori, 1997; Cong and Mitchell, 1998; Rapine et al., 2003; Hwang and Yu, 2005; Yao et al., 2005). The measured inter-station dispersion of a teleseismic surface wave can help to constrain the average Vs structures between the stations. The two selected stations and the epicenter of the teleseismic event need to be nearly on the same great-circle path. Therefore, we only select the earthquakes satisfying the two criteria: (1) the azimuthal difference of the earthquake to the two stations is less than 5°, and (2) the azimuthal difference between the earthquake to the closer station and the closer station to the farther station is less than 7° (see Fig. 12a in Yao et al., 2006). For the 7 permanent stations, there are 413 qualified teleseismic events from 2000 to 2005 with epicentral distance larger than 30° and also surface wave magnitude (Ms) above 5 (Fig. 5). We use BHZ channel (20 Hz sampling rate of vertical component) for the TS analysis.

Rayleigh waves recorded by the two stations along nearly the same great circle path from the earthquakes, after accounting for instrument response, were narrow-band-pass filtered and cross-correlated to determine the inter-station phase velocity dispersion in the period band 10–120 s using a phase velocity image analysis technique (Yao et al., 2005). Finally, after averaging all the obtained phase velocity dispersion curves for the same station-pair from all analyzed teleseismic events, we obtained the average Rayleigh wave phase velocity dispersion curve in the period band 10–120 s for each station-pair. There are only 6 station-pairs with more than 10 dispersion curves from different events (Table 1). The locations of the used teleseismic events for these 6 station-pairs are shown in Fig. 5.

5. Rayleigh wave phase velocity dispersion

Some previous studies investigated the crust and upper mantle Vs structure by a combined approach using ambient seismic noise and earthquake surface waves with regional seismic arrays (e.g., Yao et al., 2006; Yang and Ritzwoller, 2008b; Yang et al., 2008a, 2008b; Yao et al., 2008). For this study we obtained the Rayleigh wave phase velocity dispersion curve in the period band 5–120 s for each station-pair by combining dispersion data from TDEGF in the 5–30 s period band and from TS analysis in the 10–120 s period band. Following Yao et al. (2006), we require that the inter-station distance has to be at least three wavelengths for the TDEGF analysis and half of the wavelength for the TS analysis.

The measured Rayleigh wave phase velocity dispersion curves are shown for the three ideal paths (Fig. 6) and three non-ideal paths (Fig. 7) among the 6 station-pairs in Table 1 and Fig. 5. The dispersion curves for the ideal paths (Fig. 6) are almost the same at overlapping periods (10–30 s) of TDEGF and TS analysis. However, the dispersion curves for the non-ideal paths (Fig. 7) show obvious discontinuity or discrepancy at overlapping periods.

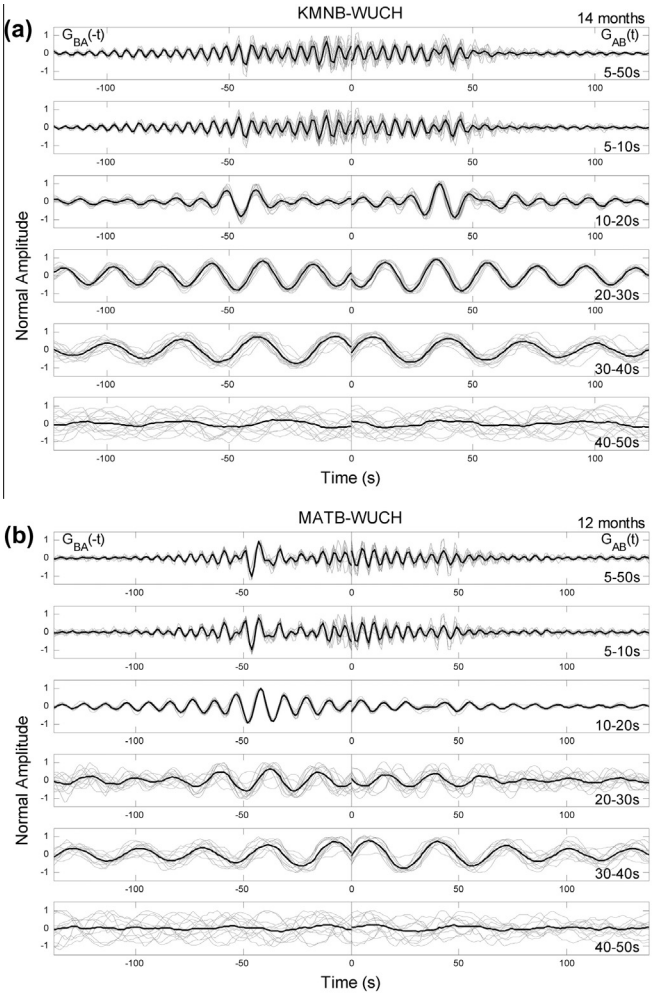

Fig. 3. TDEGFs of the two station-pairs (a) KMNB-WUCH and (b) MATB-WUCH with the temporary station WUCH. TDEGFs are band-pass filtered in six period bands and other notations are the same as Fig. 2.

This discontinuity is due to the requirement of inter-station distance which has to be at least three wavelengths for the TDEGF analysis and the phase velocity measurement at long periods is consequently restricted. This discrepancy is probably caused by a small number of events used for TS analysis for these paths (Table 1), which also results in larger standard errors of phase velocity measurements. The off-great-circle propagation and strong scattering at shorter periods for earthquake surface waves are other large potential sources of biases for TS analysis. Although the stability of monthly TDEGFs below 30 s periods (Figs. 2 and 3) indicates small errors of phase velocity measurements for ambient seismic noise analysis, we finally opted to give the same weight to TDEGF and TS measurements in the Vs inversion step. The Rayleigh wave phase velocities at overlapping periods were then obtained by averaging the results at the same period of TDEGF and TS methods.

The combined Rayleigh wave phase velocity dispersion curves of the 6 station-pairs in Figs. 6 and 7 were compared with theoretical dispersion curve of the global AK135 1-D velocity model (Kennett et al., 1995) in Fig. 8. Among these 6 station-pairs, the observed phase velocities are higher along the coastlines of Fujian Province (KMNB-MATB) and also close to the theoretical dispersion curve of the AK135 velocity model. The dispersion curves of the other 5 station-pairs are lower than AK135, especially at short periods around 10 s. In contrast to longer periods, the phase velocity variations at shorter periods of these 6 station-pairs are large, e.g., more than 0.5 km/s at periods around 10 s. Generally speaking, shorter periods sample much shallower structures which imply that lateral velocity heterogeneities in the shallow crust are larger than deeper structures in the Taiwan Strait.

Furthermore, in order to discuss lateral velocity heterogeneities in the shallow crust of the Taiwan Strait, we now focus on 5–30 s Rayleigh wave phase velocity dispersion curves of 8 station-pairs obtained from TDEGF (Fig. 9). The highest phase velocities are observed along the coastlines of Fujian Province (KMNB-MATB) and the lowest phase velocities are along the southwest offshore of Taiwan Island (PHUB-TWKB). Among the paths across the Taiwan Strait, phase velocities are about 0.1 km/s higher in the north (ANPB-MATB) and south (KMNB-PHUB) compared with the middle parts (ANPB-WUCH and RLNB-WUCH).

6. 1-D Vs structures

The 1-D crustal and upper mantle Vs structures of paths surrounding and transecting the Taiwan Strait are then inverted from the obtained Rayleigh wave phase velocity dispersion curves with Herrmann's SURF program (1987) and the Neighbourhood Algorithm (NA; Sambridge, 1999a and Sambridge, 1999b; Yao et al., 2008). For each station-pair, we first test two different initial Vs structures with SURF, that is, a half space model and a reference model. The half space structure is with Vs = 3.9 km/s, 2 km layer thickness in the upper 50 km, and 5–50 km thicker layers in the 50–200 km depth. The reference Vs model refers to the AK135 model (Kennett et al., 1995) and PREM (Dziewonski and Anderson, 1981) as well as some previous studies mentioned in Section 1.2. The layer thickness is 5 or 10 km in the upper 30 km and more than 20 km in the 30–200 km depth.

Based on the physical dispersion property of surface waves (Kanamori and Anderson, 1977), we also need to input other parameters during the Vs structures inversion. For SURF, the input density gradually increases from 2.3 g/cm^3 in the shallow crust to 3.3 g/cm^3 in the deeper crust and is set 3.3 ± 0.1 g/cm^3 in the upper mantle. The Poisson's ratio is set in the range of 0.25–0.3. For NA, the parameter settings follow Yao et al. (2008). P-wave velocity (Vp) and density structure are related to Vs using the empirical relationship from Brocher (2005) in the crust, and is perturbed with respect to Vs as described in Masters et al. (2000).

Fig. 10a takes station-pair ANPB-MATB as an example showing two different initial Vs models. No matter the half space or reference Vs model is chosen as the initial model, the final obtained Vs structures are similar and the average variance is 0.06 km/s. Since the Vs inversion cannot achieve 2 km layer thickness resolution with inter-station distances of a few hundred kilometers, we first use the SURF program to obtain the primary Vs features. Second, we choose the Vs structure from SURF as the input reference model for NA. The NA method is a two-stage procedure for nonlinear geophysical inverse problems, and is also a global searching algorithm that allows sampling almost the entire model space, and therefore should give a more robust estimate on model parameters than linearized inversions. The NA procedure follows Yao et al. (2008). There are 6 parameters: the Moho depth and Vs in 5 different non-overlapping depth intervals (0–15, 15–30, 30–75, 75–150, 150–200 km). The perturbation range of Vs is ±0.5 km/s with respect to the reference model obtained from SURF at all depth. The Moho depth is allowed to vary ±4 km with respect to the reference Moho depth, and therefore the thickness of the lower crust and uppermost mantle will also change correspondingly.

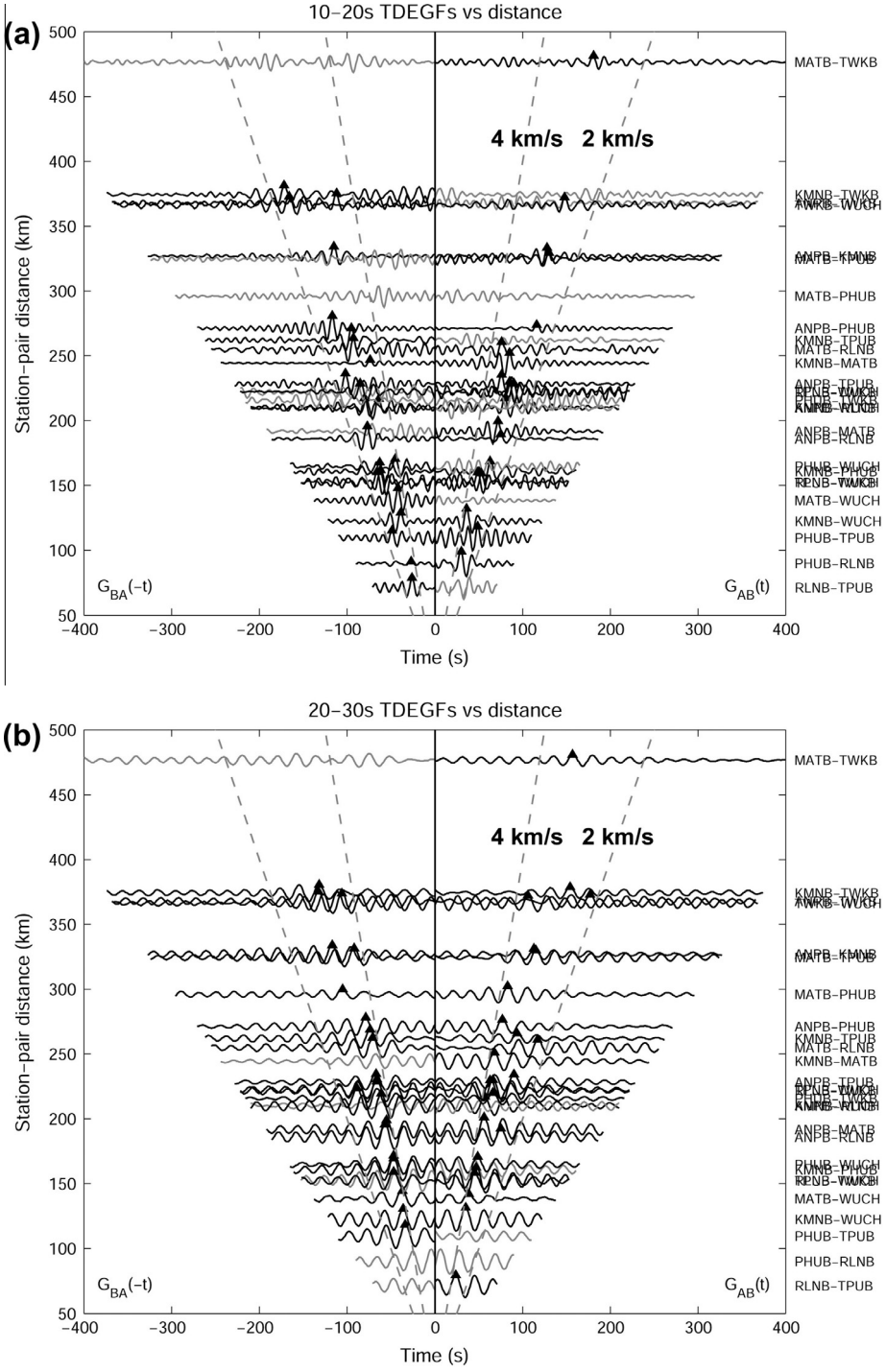

Fig. 4. All stacked TDEGFs in the period bands (a) 10–20 s and (b) 20–30 s. The station-pair names are shown on the right hand side of two sub-figures. The black triangles indicate the maximum amplitudes of TDEGFs (with +t and −t separately) with Rayleigh wave phase velocities between 2 and 4 km/s (two gray dashed lines).

Fig. 10c and d shows the Vs inversion results in the 0–200 km depth range of the 6 station-pairs in Fig. 8 from SURF and NA respectively, and which reveal very similar Vs patterns with the average variance about 0.06 km/s. Table 2 shows the discrepancy of the obtained Vs structures from SURF and NA. The largest average Vs discrepancy is 0.09 km/s along KMNB-PHUB and the smallest discrepancy is 0.03 km/s along KMNB-MATB. With respect to depth, the largest average Vs discrepancy is 0.13 km/s at 15–30 km depth probably due to the change of Moho depths during NA inversion and the smallest is 0.01 km/s at 75–150 km depth. Table 3 shows the standard errors (uncertainties) of Vs structures and Moho depths from NA. Overall speaking, the Vs standard errors are 0.07 ± 0.02 km/s for these 6 station-pairs and at 0–200 km depth, except for larger standard errors about 0.11 ± 0.03 km/s at 15–30 km depth, which are mainly due to the trade-off between Vs of this layer and the crustal thickness. The average Moho depth is 30.6 km with ±1 km variation.

Comparing Vs structures of the 6 station-pairs with the AK135 velocity model, the most obvious Vs discrepancy is in the shallow crust (Fig. 10c and d). In the shallow to middle crust (upper 15 km),

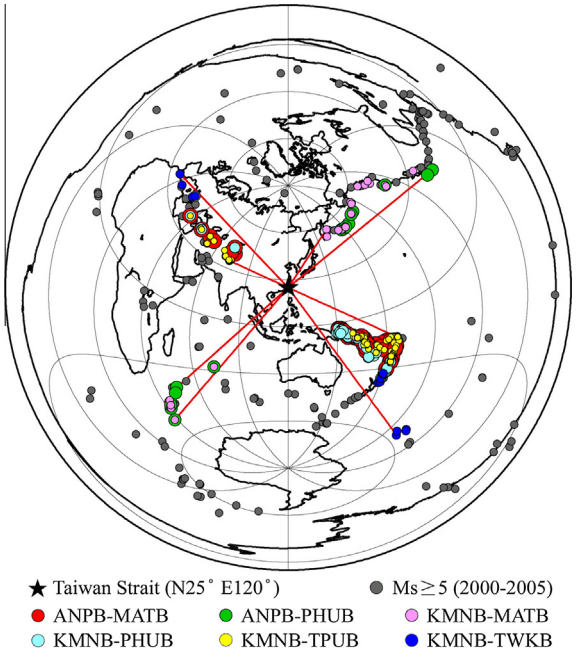

Fig. 5. The epicenter distribution (gray circles) of qualified teleseismic events occurred during the study period. The Taiwan Strait is in the center and plotted with the azimuthal equidistant projection. The circles in different colors mean the analyzed events for different station-pairs. The red lines represent great-circle paths between the analyzed events and the Taiwan Strait. (For interpretation of the references to colour in this figure legend, the reader is referred to the web version of this article.)

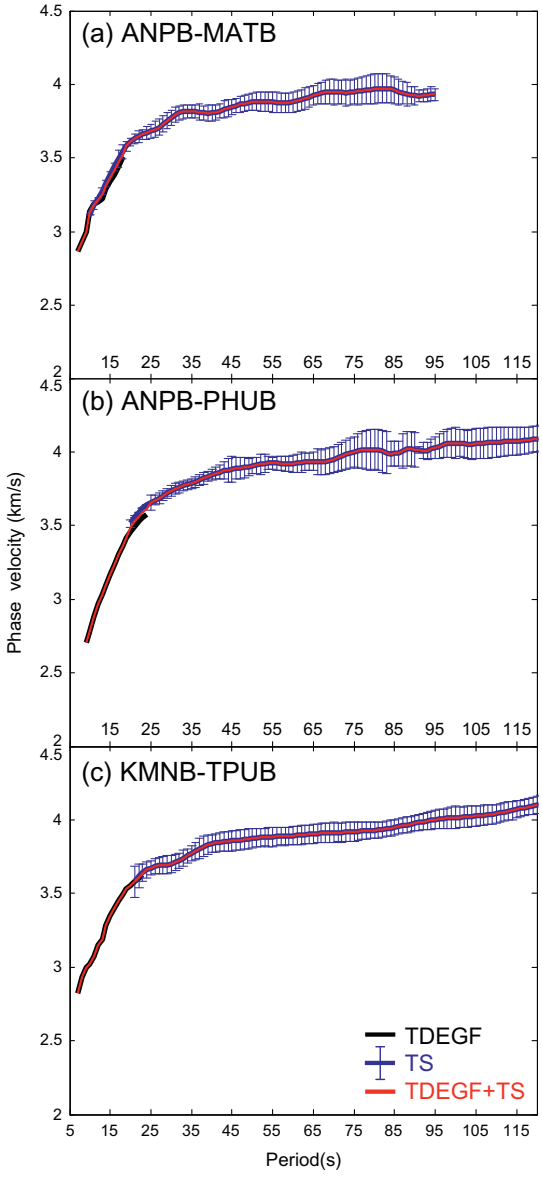

Fig. 6. The ideal Rayleigh wave phase velocity dispersion curves of three station-pairs (a) ANPB-MATB (b) ANPB-PHUB and (c) KMNB-TPUB obtained from TDEGF and TS in this study. The phase velocities at overlapping periods (10–30 s) are almost the same. The black lines are TDEGF results, the blue lines with standard errors are TS results, and the red lines are the averaging results from TDEGF and TS analyses. (For interpretation of the references to colour in this figure legend, the reader is referred to the web version of this article.)

the Vs of KMNB-MATB (close to coastlines of Fujian Province and also far away from the Taiwan orogenic belt) is the highest and more uniform, also with almost the same velocity as the AK135 model. Compared to KMNB-MATB, the Vs of KMNB-TWKB (southern Taiwan Strait) is lowest, about 1 km/s lower in the shallow crust, and 0.7 km/s lower in the middle crust. The largest velocity gradient, i.e., the Moho discontinuities of these 6 station-pairs, is at ~30 km depth and similar to the results from previous receiver function (e.g., Kao et al., 2003; Kim et al., 2004; Wang et al., 2010a, 2010b) and Bouguer gravity anomaly (Hsieh et al., 2010) studies. In the upper mantle (~30–150 km), for most paths Vs is about 0.1–0.3 km/s lower than the AK135 model. In the deeper 150–200 km depth range, Vs is in the range of ±0.2 km/s with respect to the AK135 model. Fig. 11 compares the measured Rayleigh wave phase velocity dispersion curves of the 6 station-pairs in Fig. 8 with the theoretical dispersion curves from the inverted Vs structures in Fig. 10, which shows a good fit.

From Fig. 10, the most obvious Vs discrepancy across the Taiwan Strait is in the shallow crust; also, the revealed Vs structures from SURF and NA are very consistent. Therefore, Fig. 12 focuses on the inverted Vs structures in the depth range of 0–50 km of the selected 7 station-pairs in Fig. 9 from SURF. Overall, the Vs of KMNB-MATB, far away from the Taiwan orogenic belt, is the highest. In the shallow crust (0–15 km depth), the Vs of PHUB-TWKB (southwestern offshore of the Taiwan Island) is lowest, and is 0.6–1.1 km/s lower than KMNB-MATB. Although the paths of KMNB-TWKB and KMNB-PHUB transect the southern Taiwan Strait, the Vs of KMNB-TWKB is about 0.5 km/s lower than KMNB-PHUB in the shallow crust, and is similar to PHUB-TWKB. This implies that the low Vs of KMNB-TWKB in the shallow 15 km depth is dominated by the low Vs structure along the path of PHUB-TWKB.

Table 1
The number of analyzed teleseismic events (>10) for 6 station-pairs of TS study.

Station-pair	**ANPB-MATB**	**KMNB-TPUB**	*KMNB-PHUB*	*KMNB-MATB*	**ANPB-PHUB**	*KMNB-TWKB*
Teleseismic events no.	**85**	**76**	*49*	*25*	**20**	*15*

Boldface: ideal station-pairs in Fig. 6.
Italics: non-ideal station-pairs in Fig. 7.

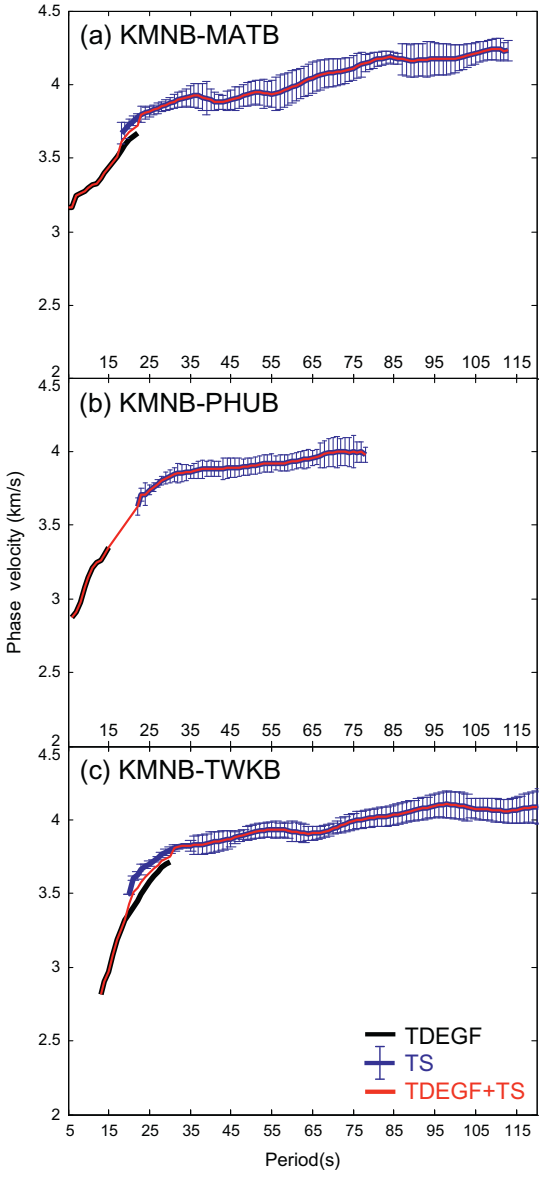

Fig. 7. Similar as Fig. 6 but for non-ideal Rayleigh wave phase velocity dispersion curves of three station-pairs (a) KMNB-MATB (b) KMNB-PHUB and (c) KMNB-TWKB obtained from TDEGF and TS in this study. The phase velocities dispersion curves show obvious discontinuous velocities at overlapping periods. (For interpretation of the references to colour in this figure legend, the reader is referred to the web version of this article.)

As mentioned in Section 5 and Fig. 9, the obtained Rayleigh wave phase velocity dispersion curve of ANPB-MATB (path which transects the northern Taiwan Strait) from TDEGF, is similar to that of KMNB-PHUB (path which transects the southern Taiwan Strait). And also the dispersion curve of ANPB-WUCH is similar to that of RLNB-WUCH (paths which transect the middle Taiwan Strait). In Fig. 12, we can compare the Vs structures of ANPB-WUCH with ANPB-MATB and KMNB-PHUB. The shallower Vs structure of ANPB-WUCH is about 0.1–0.2 km/s lower than ANPB-MATB and KMNB-PHUB down to 20 km depth. Consequently, the Vs structure across the Taiwan Strait in the shallow 20 km depth range is slightly (about 0.1–0.2 km/s) lower in the middle section than in the northern and southern sections.

Among the 7 selected station-pairs in Fig. 12, the path of ANPB-TWKB is different from the others transecting the Taiwan Strait, but across the main geologic axis of the Taiwan Island, the Vs structure is also different. In the shallow 10 km range, the Vs of ANPB-TWKB is 0.2 km/s lower than KMNB-MATB and is 0.1–0.9 km/s higher than the other paths transecting the Taiwan Strait. The possible Moho depth is ~35 km or even 45 km for ANPB-TWKB, deeper than the other station-pairs with ~30 km Moho depths. This discrepancy of Moho depths was also observed in other recent studies (e.g., Kim et al., 2004; Hsieh et al., 2010; Wang et al., 2010a).

7. Discussion

Overall, the Vs structures and velocity patterns across the Taiwan Strait in this study compare well with previous studies, e.g., from receiver functions and the Bouguer gravity anomaly mentioned in Section 1.2. The path KMNB-MATB is the farthest away from the Taiwan orogeny and has the highest Vs along it. In the shallow crust, the Vs of PHUB-TWKB is lowest in southwest offshore of Taiwan Island, and the Vs in the middle section of the Taiwan Strait is slightly lower than the northern and southern sections. The velocity patterns compare well with the thickness of Cenozoic sedimentary foreland basin (Lin et al., 2003). The lowest Vs in southwestern offshore of Taiwan Island corresponds to 10–14 km thick Tainan Basin, and the low Vs in the middle sections of the Taiwan Strait also corresponds to 6–8 km thick Taihsi Basin (Figs. 1 and 12a). Previous velocity structure studies in the Taiwan region (e.g., Kim et al., 2005; Wu et al., 2007; Kuo-Chen et al., 2012) also showed remarkable low velocities southwest of Taiwan Island.

The thick Cenozoic sedimentary foreland basin definitely plays an important role to contribute the obtained low Vs structures in southwest offshore of Taiwan Island (PHUB-TWKB) in the shallow crust. Besides, deeper bathymetry than the average water depth (less than 50 m) of the Taiwan Strait (Fig. 1) may also affect Rayleigh wave phase velocity measurements at the short periods. In Fig. 13, we use the Rayleigh wave phase velocity dispersion curve of PHUB-TWKB from TDEGF as an example and show how a water layer with various thicknesses will affect phase velocities at shorter periods. The parameters of water layer referring to AK135 and PREM: Vp = 1.45 km/s, Vs = 0 km/s, density = 1.02 g/cm^3, and Poisson's ratio = 0.5. The top 5 km crustal structure is replaced by the water layer gradually. For instance, if the water layer is 1 km thick, then the thickness of the uppermost crustal layer is reduced to 4 km. As presented in Fig. 13, it shows that 50 m thick water layer (average water depth of the Taiwan Strait) nearly does not affect the dispersion curve. But when the water layer becomes thicker than 1000 m, the difference becomes obvious. When the water layer is 1000 m thick, Rayleigh wave phase velocity dispersion at 5 s is about 0.12 km/s lower than that without a water layer. Similarly, the Rayleigh wave phase velocity at 5 s appears 0.38 and 0.61 km/s lower with a 2000 and a 3000 m thick water layer, respectively. As a result, seismic velocity inversion using shorter period band dispersion data in the sea areas with water depth deeper than 1000 m should take water layer into account except the studies in the continental shelves.

We found the Moho discontinuity depths are about 30 km across the Taiwan Strait, and 35–45 km for ANPB-TWKB across the main geologic axis of Taiwan Island. These results are consistent with various studies (e.g., Kim et al., 2005; Wu et al., 2007; Hsieh et al., 2010; Wang et al., 2010a; Kuo-Chen et al., 2012). The crustal thickness beneath the Backbone Range of Taiwan Island even reaches 55–60 km as mountain root mentioned in some previous studies. Hwang and Yu (2005) analyzed Rayleigh wave phase velocity dispersion to derive a 200 km deep Vs structure under the Taiwan Island. Their crustal thickness beneath the Backbone Range is 40–50 km which is slightly thicker than ours (35–45 km) and

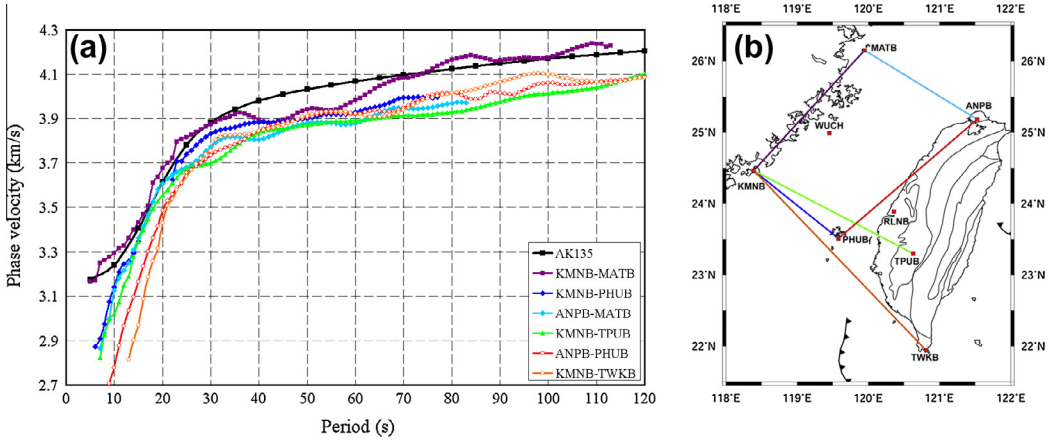

Fig. 8. (a) Rayleigh wave phase velocity dispersion curves in the period band 5–120 s of 6 station-pairs obtained from TDEGF and TS in this study compared with the theoretical dispersion curve of AK135 velocity model. (b) The paths of the selected station-pairs. (For interpretation of the references to colour in this figure legend, the reader is referred to the web version of this article.)

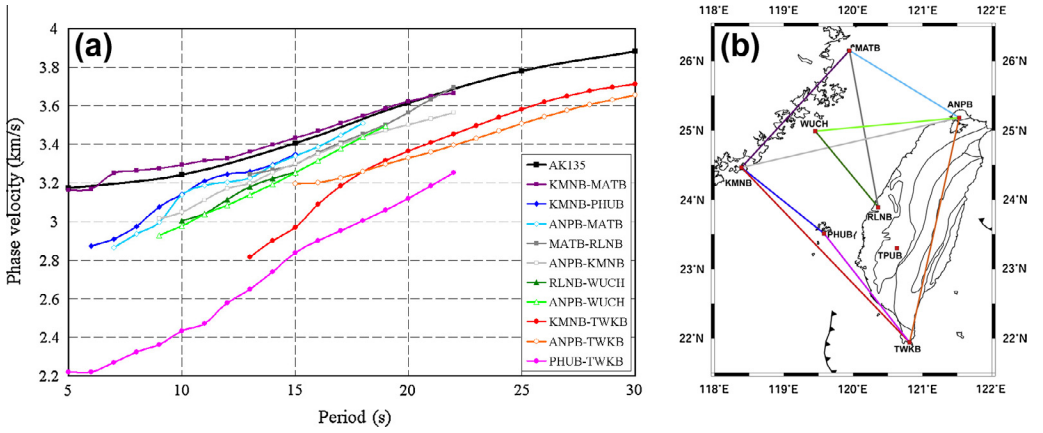

Fig. 9. (a) The Rayleigh wave phase velocity dispersion curves in the period band 5–30 s of 8 station-pairs obtained from TDEGF in this study compared with the theoretical dispersion curve of AK135 velocity model. (b) The paths of the selected station-pairs. (For interpretation of the references to colour in this figure legend, the reader is referred to the web version of this article.)

much thicker than the Taiwan Strait (~30 km). They obtained an upper mantle low velocity zone with Vs of 4.25–4.4 km/s at around 100 km depth under the Taiwan Island. Our Vs structures beneath the Taiwan Strait (Fig. 10) also reveal similar features, which imply that the upper mantle low Vs zone generally exists beneath and around the Taiwan regions. Consequently, the significant differences of the Vs structures across the Taiwan Strait are in the shallow crust and the Taiwan Strait also shows relatively a thinner crust and simpler tectonic structures than the Taiwan Island.

The persistent localized microseismic sources may lead TDEGF fail to approximate the true Green's function. Zeng and Ni (2010, 2011) studied TDEGF in East Asia and found persistent strong signals with higher apparent velocity than Rayleigh waves. The microseismic sources were suspected from volcanism activities and located beneath Aso volcano on Kyushu Island, Japan. Zheng et al. (2011) performed ambient noise tomography in North China and found that when the arrival times of the volcanic signals are close to expected surface waves, it is difficult to separate these two signals and this may affect dispersion measurements from the TDEGF. Hence, they did a simple correction to eliminate the effect of the volcanic microseism on the dispersion measurements. However, the Taiwan Strait is about 1500 kilometers away from the Kyushu Island. It is also noteworthy that there are some volcanism activities around northern Taiwan, the Tatun Volcano Group (e.g., Lin et al., 2005a, 2005b; Konstantinou et al., 2007) and Kueishantao Island (e.g., Konstantinou et al., 2013). The major energy of volcanic microseism around northern Taiwan is concentrated at 1–20 Hz, outside the 5–120 s (0.008–0.2 Hz) period band in this study. In Fig. 4, the dominant signals are mainly expected Rayleigh waves and no other obviously persistent strong signals as Zeng and Ni (2010, 2011) and Zheng et al. (2011) observed in North China. Zhou et al. (2012) conducted ambient noise and earthquake surface wave tomography in South China beside the Taiwan Strait and they did not observe other persistent signals, neither.

An earthquake surface wave two-station analysis is a simple and traditional method to explore regional crust and upper mantle Vs structures. But there are some inherent limitations that may influence the accuracy of the measured results, especially at short periods around 10–30 s, i.e., the overlapping periods in this study. In order to obtain more stable and reliable Vs structures between the station-pairs, the attempt to analyze more earthquake surface wave records is usually put into practice. But due to the restrictions of global seismicity and the orientations of station-pairs, it is difficult to select enough teleseismic events on the same great-circle path for some station-pairs. Yao et al. (2006) discussed the

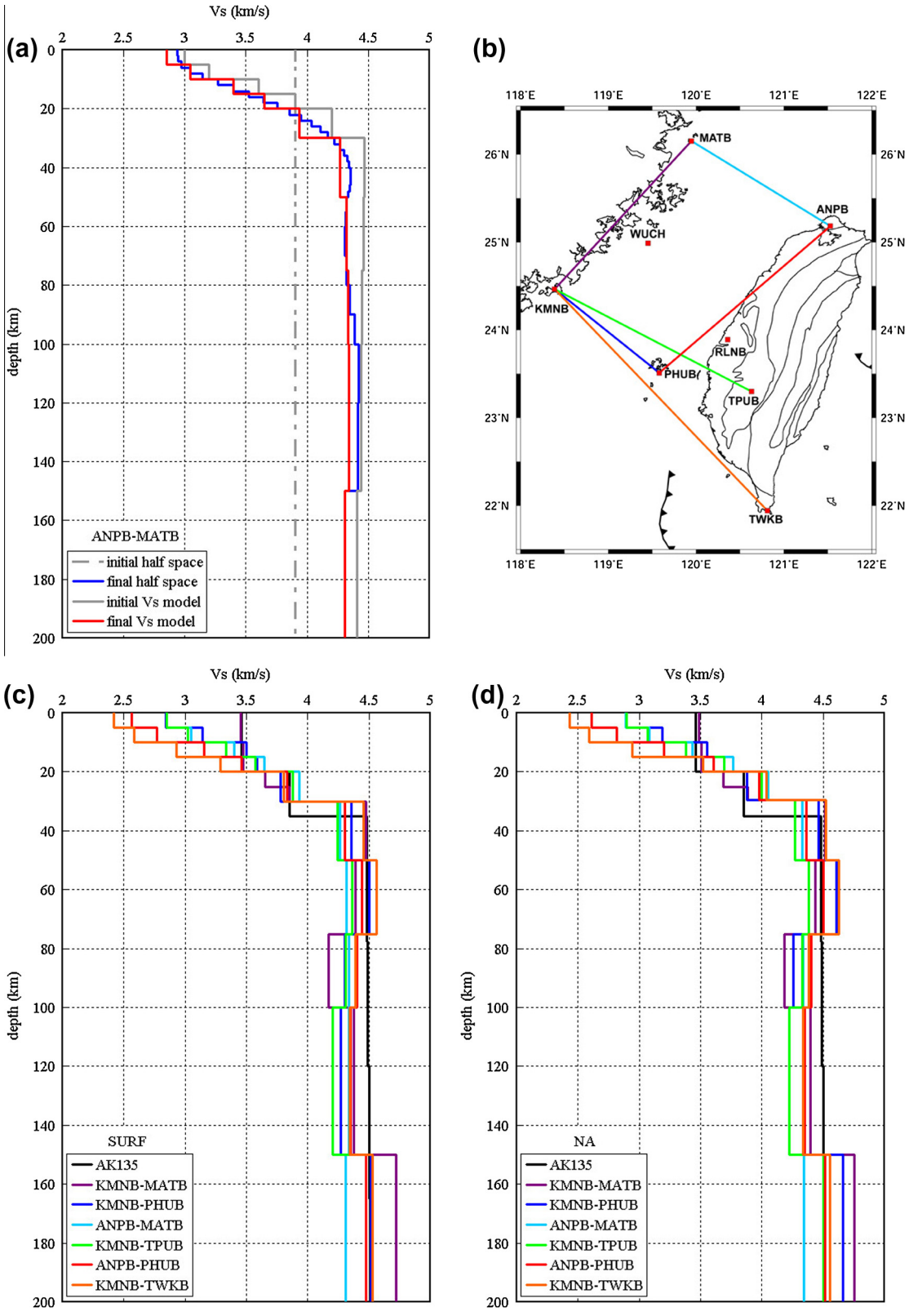

Fig. 10. The inversion results of Vs structures in the crust and upper mantle (0–200 km depth) of the 6 station-pairs in Fig. 8. (a) Taking ANPB-KMNB as an example to show two different initial velocity models in SURF both lead to similar inversion results. (b) The paths of the selected station-pairs. (c) The obtained Vs structures from SURF. (d) The obtained Vs structures from NA. (For interpretation of the references to colour in this figure legend, the reader is referred to the web version of this article.)

possible sources of inaccuracy for the TS method, such as scattering effect, off-great-circle propagation, the influence of velocity anomaly along propagation path, different sensitivity zones between TDEGF and TS measurements. Yao et al. (2006) found that the TS method gives about 1–3% higher than phase velocity measurements than the TDEGF results in the overlapping periods (20–30 s). Some of two-station paths in this study also show similar results (Figs. 6 and 7). For the ambient seismic noise method, the

Table 2
The discrepancy of obtained Vs structures of the 6 station-pairs for the 5 non-overlapping depth intervals from SURF and NA (unit: km/s).

Depth (km)	KMNB-MATB	KMNB-PHUB	ANPB-MATB	KMNB-TPUB	ANPB-PHUB	KMNB-TWKB	Average
0–15	0.03	0.05	0.04	0.05	0.05	0.01	0.04
15–30	0.03	0.10	0.12	0.12	0.14	0.23	0.13
30–75	0.04	0.11	0.07	0.02	0.06	0.07	0.06
75–150	0.01	0.05	0.00	0.02	0.00	0.01	0.01
150–200	0.03	0.15	0.03	0.02	0.04	0.02	0.05
Average	0.03	0.09	0.05	0.05	0.06	0.07	0.06

Table 3
The standard errors (uncertainties) of obtained Vs structures of the 6 station-pairs for the 5 non-overlapping depth intervals from NA (unit: km/s). The last raw shows the Moho depth (km) obtained from NA.

Depth (km)	KMNB-MATB	KMNB-PHUB	ANPB-MATB	KMNB-TPUB	ANPB-PHUB	KMNB-TWKB	Average
0–15	0.05	0.05	0.05	0.06	0.06	0.07	0.06
15–30	0.14	0.08	0.08	0.09	0.10	0.12	0.11
30–75	0.08	0.07	0.06	0.06	0.07	0.09	0.07
75–150	0.06	0.06	0.05	0.06	0.06	0.06	0.06
150–200	0.05	0.11	0.06	0.06	0.06	0.06	0.06
Average	0.08	0.08	0.06	0.07	0.07	0.08	0.07
Moho	29.6	31.6	31.4	30.3	30.1	30.3	30.6

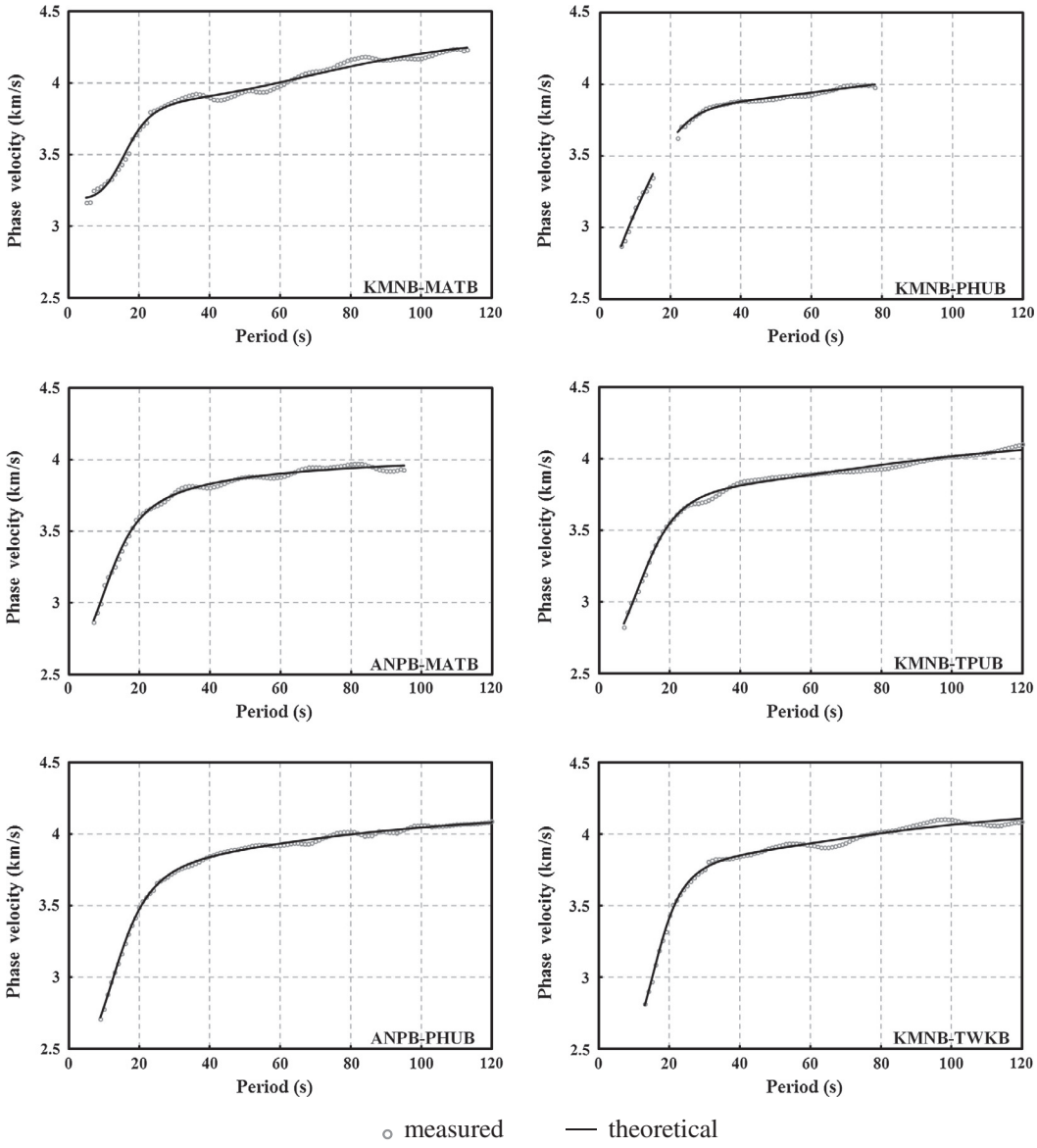

Fig. 11. Comparing the theoretical (from inverted Vs structures in Fig. 10) and measured (Fig. 8) Rayleigh wave phase velocity dispersion curves of the 6 station-pairs.

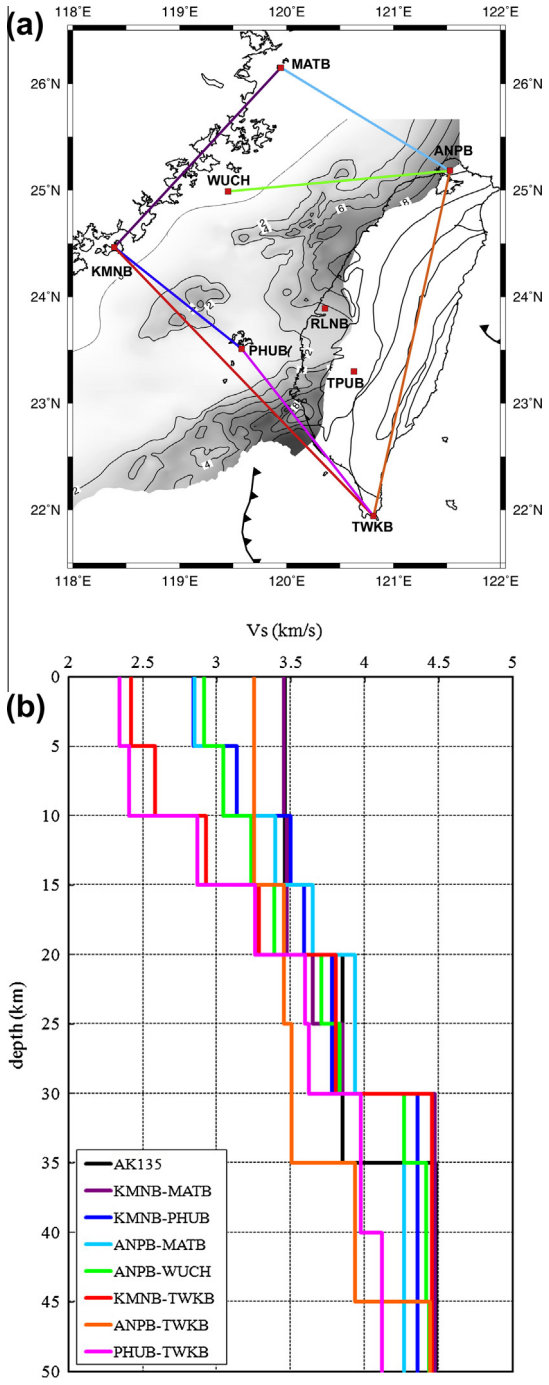

Fig. 12. The Vs inversion results in the 0–50 km depth ranges of the 7 station-pairs in Fig. 9. (a) The paths of the selected station-pairs. Cenozoic sedimentary foreland basins in the Taiwan Strait are from Lin et al. (2003). (b) The obtained Vs structures from SURF. (For interpretation of the references to colour in this figure legend, the reader is referred to the web version of this article.)

uneven distribution of noise sources may bias the phase velocity measurements (e.g., Yao and Van der Hilst, 2009; Tsai, 2009). This bias is typically within 1% of the measured phase velocities (Yao and Van der Hilst, 2009) if the azimuthal variation of the ambient seismic noise energy is smooth.

However, with proper suppression of the finite frequency effect of the earthquake two-station analysis and with more earthquake-based measurements, Yao et al. (2010) showed a generally consistent phase velocity dispersion measurements between the TDEGF and TS methods in the overlapping 20–40 s period band. The phase velocity maps derived from the ambient seismic noise and the teleseismic surface-wave two-plane wave methods in the overlapping periods appear also consistent, e.g., in the western US (Yang and Ritzwoller, 2008b) and south Africa (Yang et al., 2008a). Therefore, the combination of the dispersion data from the ambient seismic noise and the earthquake-based surface wave methods is generally reliable to obtain the Vs structure from the upper crust to upper mantle as we did in this study.

We obtained 1-D Vs structures across the Taiwan Strait from ambient seismic noise and earthquake surface wave signals recorded by broadband stations operated by IESAS. Further high-resolution studies in this region can be achieved with more broadband stations surrounding the Taiwan Strait, for instance, from some comprehensive projects like TAICRUST and TAIGER and from broadband arrays in Fujian province of Mainland China.

8. Conclusions

We selected 7 permanent stations and one temporary station operated by IESAS on both sides of the Taiwan Strait to study 1-D average Vs structures between some station-pairs by analyzing ambient seismic noise and earthquake surface wave signals. The obtained 5–120 s inter-station Rayleigh wave phase velocity dispersion curves were the average results from TDEGFs at 5–30 s and from TS at 10–120 s, which were then used to invert for Vs structures in the crust and upper mantle.

The seismic velocity inversion studies using shorter period band dispersion data in the sea areas with water depth deeper than 1000 m should take water layer into consideration except for the continental shelves. The obtained 1-D Vs structures compare well with previous studies. The significant differences of the Vs structures across the Taiwan Strait are in the shallow 15 km crust. The highest Vs in the upper crust is observed along the coastlines of Mainland China (KMNB-MATB), which is far from the collision zone of Taiwan orogenic belt, similar to the AK135 upper crust velocity model. Conversely, the lowest Vs in the upper crust appears along southwestern offshore of Taiwan Island (PHUB-TWKB), which is 0.6–1.1 km/s lower than KMNB-MATB. The upper crustal Vs structure in the middle section of the Taiwan Strait is 0.1–0.2 km/s lower than the northern and southern sections. The upper mantle Vs structure (Moho–150 km) beneath the Taiwan Strait is about 0.1–0.3 km/s lower than the AK135 model. The Moho discontinuity depths are 30 km across the Taiwan Strait, and showing relatively thinner crust and simpler tectonic structures than Taiwan Island.

Acknowledgments

The authors would like to thank an anonymous reviewer and the Editor for constructive comments for improving the manuscript. Jeen-Hwa Wang, Ban-Yuan Kuo, Tao-Ming Chang, Ruey-Der Hwang, Kuo-En Ching, Chung-Han Chan, and Kesong Wan gave constructive suggestions of the manuscript. The members of Taiwan Volcano Observatory-Tatun (TVO) kindly helped in revising the manuscript. The data used in this research were collected by the Institute of Earth Sciences, Academia Sinica. This research was supported by the Institute of Earth Sciences, Academia Sinica and National Science Council under Grant Numbers NSC 99-2116-M-001-022 and NSC 99-2116-M-001-026. This research is also supported by the National Natural Science Foundation of China (#41222028) to Huajian Yao and the Chinese Academy of Sciences/State Administration of Foreign Experts Affairs International Partnership Program for Creative Research Teams.

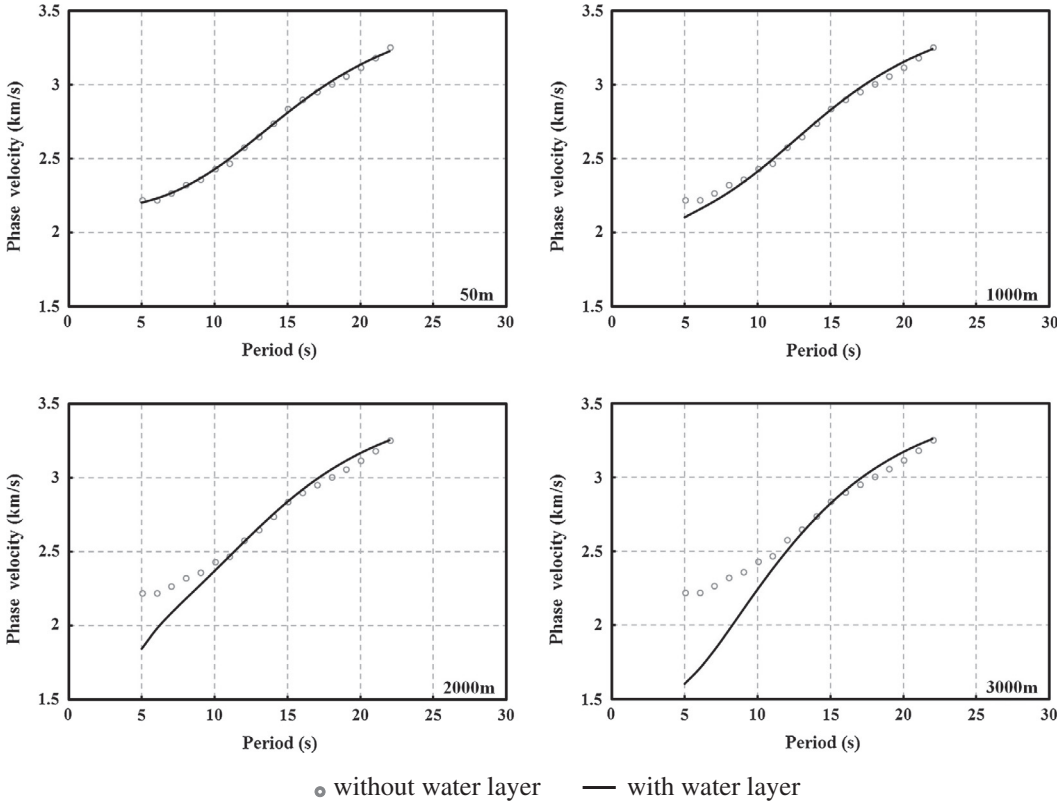

Fig. 13. Comparison of synthetic Rayleigh wave phase velocity dispersion curves of PHUB-TWKB with four different water layer thicknesses.

References

Ai, Y., Chen, Q., Zeng, F., Hong, X., Ye, W., 2007. The crust and upper mantle structure beneath southeastern China. Earth Planet. Sci. Lett. 260, 549–563.

Angelier, J., 1986. Geodynamics of the Eurasia-Philippine Sea plate boundary: preface. Tectonophysics 125, IX–X.

Bensen, G.D., Ritzwoller, M.H., Shapiro, N.M., 2008. Broadband ambient noise surface wave tomography across the United States. J. Geophys. Res. 113, B05306.

Bensen, G.D., Ritzwoller, M.H., Yang, Y., 2009. A 3-D shear velocity model of the crust and uppermost mantle beneath the United States from ambient seismic noise. Geophys. J. Int. 177, 1177–1196.

Brocher, T.M., 2005. Empirical relations between elastic wavespeeds and density in the Earth's crust. Bull. Seismol. Soc. Am. 95, 2081–2092.

Bromirski, P.D., 2001. Vibrations from the "Perfect Storm". Geochemistry, Geophysics, Geosystems, vol. 2, 2000GC000119.

Chen, C.H., Chen, Y.H., Yen, H.Y., Yu, G.K., 2003. Lateral variations of Pn velocity and anisotropy in Taiwan from travel-time tomography. Earth, Planets Space 55, 223–230.

Cho, K.H., Herrmann, R.B., Ammon, C.J., Lee, K., 2007. Imaging the upper crust of the Korean Peninsula by surface-wave tomography. Bull. Seismol. Soc. Am. 97, 198–207.

Cong, L., Mitchell, B.J., 1998. Seismic velocity and *Q* structure of the Middle Eastern crust and upper mantle from surface-wave dispersion and attenuation. Pure Appl. Geophys. 153, 503–538.

Cupillard, P., Capdeville, Y., 2010. On the amplitude of surface waves obtained by noise correlation and the capability to recover the attenuation: a numerical approach. Geophys. J. Int. 181, 1687–1700.

Dziewonski, A.M., Anderson, D.L., 1981. Preliminary reference Earth model. Phys. Earth Planet. Inter. 25, 297–356.

Goldstein, P., Dodge, D., Firpo, M., Minner, L., 2003. In: Lee, W.H.K., Kanamori, H., Jennings, P.C., Kisslinger, C. (Eds.), SAC2000: Signal Processing and Analysis Tools for Seismologists and Engineers, Invited Contribution to The IASPEI International Handbook of Earthquake and Engineering Seismology. Academic Press, London.

Harmon, N., Forsyth, D., Webb, S., 2007. Using ambient seismic noise to determine short-period phase velocities and shallow shear velocities in young oceanic lithosphere. Bull. Seismol. Soc. Am. 97, 2009–2023.

Herrmann, R.B., 1987. Computer Programs in Seismology, User's Manual, IV, St. Louis University, St. Louis, Missouri.

Ho, C.S., 1988. An introduction to the geology of Taiwan: explanatory text of the geologic map of Taiwan (second ed.). Central Geological Survey, Ministry of Economic Affairs, Taiwan, 192 pp.

Hsieh, H.H., Yen, H.Y., Shih, M.H., 2010. Moho depth derived from gravity data in the Taiwan Strait area. Terr., Atmos. Ocean. Sci. 21, 235–241.

Hsu, S.K., Sibuet, J.C., 1995. Is Taiwan the result of arc-continent or arc-arc collision? Earth Planet. Sci. Lett. 136, 315–324.

Hsu, Y.J., Yu, S.B., Simons, M., Kuo, L.C., Chen, H.Y., 2009. Interseismic crustal deformation in the Taiwan plate boundary zone revealed by GPS observations, seismicity, and earthquake focal mechanisms. Tectonophysics 479, 4–18.

Huang, B.S., Chen, K.C., Wang, K.L., Yen, H.Y., 1998. Velocities of Pn-waves in the Taiwan Strait and its surrounding area from regional earthquakes. Terr., Atmos. Ocean. Sci. 9, 473–486.

Huang, B.S., Chen, K.C., Yen, H.Y., Yao, Z.X., 1999. Re-examination of the epicenter of the 16 September 1994 Taiwan Strait erthquake using the beam-forming method. Terr., Atmos. Ocean. Sci. 10, 529–542.

Huang, T.Y., Gung, Y., Liang, W.T., Chiao, L.Y., 2012. Broad-band Rayleigh wave tomography of Taiwan and its implications on gravity anomalies. Geophys. Res. Lett. 39, L05305.

Huang, Y.C., Yao, H., Huang, B.S., van der Hilst, R.D., Wen, K.L., Huang, W.G., Chen, C.H., 2010a. Phase velocity variation at periods of 0.5–3.0 s in the Taipei Basin of Taiwan from correlation of ambient seismic noise. Bull. Seismol. Soc. Am. 100, 2250–2263.

Huang, Z., Wang, L., Zhao, D., Xu, M., Mi, N., Yu, D., Li, H., Li, C., 2010b. Upper mantle structure and dynamics beneath Southern China. Phys. Earth Planet. Inter. 182, 161–169.

Hwang, R.D., Yu, G.K., 2005. Shear-wave velocity structure of upper mantle under Taiwan from the array analysis of surface waves. Geophys. Res. Lett. 32, L07310.

Kanamori, Hiroo., Anderson, D.L., 1977. Importance of physical dispersion in surface wave and free oscillation problems: review. Rev. Geophys. 15, 105–112.

Kang, T.S., Shin, J.S., 2006. Surface-wave tomography from ambient seismic noise of accelerograph networks in southern Korea. Geophys. Res. Lett. 33, L17303.

Kao, H., Wu, F.T., 1996. The 16 September 1994 earthquake (m_b = 6.5) in the Taiwan Strait and its tectonic implications. Terr., Atmos. Ocean. Sci. 7, 13–29.

Kao, H., Jian, P.R., Ma, K.F., Huang, B.S., Liu, C.C., 1998. Moment-tensor inversion for offshore earthquakes east of Taiwan and their implications to regional collision. Geophys. Res. Lett. 25, 3619–3622.

Kao, H., Chang, C.H., Chen, R.Y., 2003. Receiver function analysis for broadband stations in Taiwan. Technical Report of Seismology Center, Central Weather Bureau (Taiwan), vol. 33, pp. 88–136.

Kennett, B.L.N., Engdahl, E.R., Buland, R., 1995. Constraints on seismic velocities in the Earth from traveltimes. Geophys. J. Int. 122, 108–124.

Kim, K.H., Chiu, J.M., Kao, H., Liu, Q., Yeh, Y.H., 2004. A preliminary study of crustal structure in Taiwan region using receiver function analysis. Geophys. J. Int. 159, 146–164.

Kim, K.H., Chiu, J.M., Pujol, J., Chen, K.C., Huang, B.S., Yeh, Y.H., Shen, P., 2005. Three-dimensional Vp and Vs structural models associated with the active subduction and collision tectonics in the Taiwan region. Geophys. J. Int. 162, 204–220.
Konstantinou, K.I., Lin, C.H., Liang, W.T., 2007. Seismicity characteristics of a potentially active Quarternary volcano: the Tatun Volcano Group, northern Taiwan. J. Volcanol. Geoth. Res. 160, 300–318.
Konstantinou, K.I., Pan, C.Y., Lin, C.H., 2013. Microearthquake activity around Kueishantao island, offshore northeastern Taiwan: insights into the volcano-tectonic interactions at the tip of the southern Okinawa Trough. Tectonophysics 593, 20–32.
Kuo-Chen, H., Wu, F.T., Roecker, S.W., 2012. Three-dimensional P velocity structures of the lithosphere beneath Taiwan from the analysis of TAIGER and related seismic data sets. J. Geophys. Res. 117, B06306.
Larose, E., Derode, A., Campillo, M., Fink, M., 2004. Imaging from one-bit correlations of wideband diffuse wave fields. J. Appl. Phys. 95, 8393–8399.
Lee, W.H.K., Wu, F.T., Jacobsen, C., 1976. A catalog of historical earthquakes in China compiled from recent Chinese publications. Bull. Seismol. Soc. Am. 66, 2003–2016.
Li, H., Bernardi, F., Michelini, A., 2010. Surface wave dispersion measure-ments from ambient seismic noise analysis in Italy. Geophys. J. Int. 180, 1242–1252.
Li, H., Su, W., Wang, C.Y., Huang, Z., 2009. Ambient noise Rayleigh wave tomography in western Sichuan and eastern Tibet. Earth Planet. Sci. Lett. 282, 201–211.
Liang, W.T., Liu, Y.H., Kao, H., 2004. Source parameters of regional earthquakes in Taiwan: January–December, 2002. Terr., Atmos. Ocean. Sci. 15, 727–741.
Lin, A.T., Watts, A.B., 2002. Origin of the West Taiwan basin by orogenic loading and flexure of a rifted continental margin. J. Geophys. Res. 107, 2185.
Lin, A.T., Watts, A.B., Hesselbo, S.P., 2003. Cenozoic stratigraphy and subsidence history of the South China Sea margin in the Taiwan region. Basin Res. 15, 453–478.
Lin, C.H., 2000. Thermal modeling of continental subduction and exhumation constrained by heat flow and seismicity in Taiwan. Tectonophysics 324, 189–201.
Lin, C.H., 2002. Active continental subduction and crustal exhumation: the Taiwan orogeny. Terra Nova 14, 281–287.
Lin, C.H., Konstantinou, K.I., Liang, W.T., Pu, H.C., Lin, Y.M., You, S.H., Huang, Y.P., 2005a. Preliminary analysis of volcano seismic signals recorded at the Tatun Volcano Group, northern Taiwan. Geophys. Res. Lett. 32, L10313.
Lin, C.H., Konstantinou, K.I., Pu, H.C., Hsu, C.C., Lin, Y.M., You, S.H., Huang, Y.P., 2005b. Preliminary results from seismic monitoring at Tatun volcanic area of northern Taiwan. Terr., Atmos. Ocean. Sci. 16, 563–577.
Lin, F.C., Ritzwoller, M.H., Shapiro, N.M., 2006. Is ambient noise tomography across ocean basins possible? Geophys. Res. Lett. 33, L14304.
Lin, F.C., Ritzwoller, M.H., Townend, J., Bannister, S., Savage, M.K., 2007. Ambient noise Rayleigh wave tomography of New Zealand. Geophys. J. Int. 170, 649–666.
Lin, F.C., Moschetti, M.P., Ritzwoller, M.H., 2008. Surface wave tomography of the western United States from ambient seismic noise: Rayleigh and Love wave phase velocity maps. Geophys. J. Int. 173, 281–298.
Ma, K.F., Wang, J.H., Zhao, D., 1996. Three-dimensional seismic velocity structure of the crust and uppermost mantle beneath Taiwan. J. Phys. Earth 44, 85–105.
Marzorati, S., Bindi, D., 2008. Characteristics of ambient noise cross correlations in northern Italy within the frequency range of 0.1–0.6 Hz. Bull. Seismol. Soc. Am. 98, 1389–1398.
Masters, G., Laske, G., Bolton, H., Dziewonski, A., 2000. The relative behavior of shear velocity, bulk sound speed, and compressional velocity in the mantle: implications for chemical and thermal structure. Geophys. Monogr. Ser. 117, 63–87.
McIntosh, K., Nakamura, Y., Wang, T.K., Shih, R.C., Chen, A., Liu, C.S., 2005. Crustal-scale seismic profiles across Taiwan and the western Philippine Sea. Tectonophysics 401, 23–54.
Nakamura, Y., McIntosh, K., Chen, A.T., 1998. Preliminary results of a large offset seismic survey west of Hengchun Peninsula, southern Taiwan. Terr., Atmos. Ocean. Sci. 9, 395–408.
Polet, J., Kanamori, H., 1997. Upper-mantle shear velocities beneath Southern California determined from Long-period surface waves. Bull. Seismol. Soc. Am. 87, 200–209.
Rapine, R., Tilmann, F., West, M., Ni, J., Rodgers, A., 2003. Crustal structure of northern and southern Tibet from surface wave dispersion analysis. J. Geophys. Res. 108, 2120.
Rau, R.J., Wu, F.T., 1995. Tomography imaging of lithospheric structure under Taiwan. Earth Planet. Sci. Lett. 133, 517–532.
Roecker, S.W., Yeh, Y.H., Tsai, Y.B., 1987. Three-dimensional P and S wave velocity structures beneath Taiwan: deep structure beneath an arc-continent collision. J. Geophys. Res. 92, 10547–10570.
Sabra, K.G., Gerstoft, P., Roux, P., Kuperman, W.A., Fehler, M.C., 2005a. Extracting time-domain Green's function estimates from ambient seismic noise. Geophys. Res. Lett. 32, L03310.
Sabra, K.G., Gerstoft, P., Roux, P., Kuperman, W.A., Fehler, M.C., 2005b. Surface wave tomography from microseisms in Southern California. Geophys. Res. Lett. 32, L14311.
Sambridge, M., 1999a. Geophysical inversion with a neighbourhood algorithm – I. Searching a parameter space. Geophys. J. Int. 138, 479–494.
Sambridge, M., 1999b. Geophysical inversion with a neighbourhood algorithm – II: Appraising the ensemble. Geophys. J. Int. 138, 727–746.
Saygin, E., Kennett, B.L.N., 2010. Ambient seismic noise tomography of Australian continent. Tectonophysics 481, 116–125.
Seno, T., Kawanishi, Y., 2009. Reappraisal of the arc-arc collision in Taiwan. Terr., Atmos. Ocean. Sci. 20, 573–585.
Seno, T., Stein, S., Gripp, A.E., 1993. A model for the motion of the Philippine Sea plate consistent with NUVEL-1 and geological data. J. Geophys. Res. 98, 17941–17948.
Shapiro, N.M., Campillo, M., 2004. Emergence of broadband Rayleigh waves from correlations of the ambient seismic noise. Geophys. Res. Lett. 31, L07614.
Shapiro, N.M., Campillo, M., Stehly, L., Ritzwoller, M.H., 2005. High-resolution surface-wave tomography from ambient seismic noise. Science 307, 1615–1618.
Shih, R.C., Lin, C.H., Lai, H.L., Yeh, Y.H., Huang, B.S., Yen, H.Y., 1998. Preliminary crustal structures across central Taiwan from modeling of the onshore-offshore wide-angle seismic data. Terr., Atmos. Ocean. Sci. 9, 317–328.
Sibuet, J.C., Hsu, S.K., 1997. Geodynamics of the Taiwan arc-arc collision. Tectonophysics 274, 221–251.
Stehly, L., Campillo, M., Shapiro, N.M., 2006. A study of the seismic noise from its long-range correlation properties. J. Geophys. Res. 111, B10306.
Stehly, L., Fry, B., Campillo, M., Shapiro, N.M., Guilbert, J., Boschi, L., Giardini, D., 2009. Tomography of the Alpine region from observations of seismic ambient noise. Geophys. J. Int. 178, 338–350.
Suppe, J., 1981. Mechanics of mountain building and metamorphism in Taiwan. Memoir Geol. Soc. China 4, 67–89.
Teng, L.S., 1990. Geotectonic evolution of late Cenozoic arc-continent collision in Taiwan. Tectonophysics 183, 57–76.
Traer, J., Gerstoft, P., Bromirski, P.D., Hodgkiss, W.S., Brooks, L.A., 2008. Shallow-water seismoacoustic noise generated by tropical storms Ernesto and Florence. J. Acoust. Soc. Am. 124, EL170–EL176.
Tsai, Y.B., 1986. Seismotectonics of Taiwan. Tectonophysics 125, 17–37.
Tsai, V.C., 2009. On establishing the accuracy of noise tomography travel-time measurements in a realistic medium. Geophys. J. Int. 178, 1555–1564.
Wang, C.Y., Yen, H.Y., Leu, P.L., Chang, C.H., 2011. The explorations of the Moho discontinuities beneath Taiwan. In: Conference on Weather Analysis, Forecasting and Seismic Observation, Central Weather Bureau (Taiwan), pp. 10–16. (in Chinese).
Wang, H.L., Chen, H.W., Zhu, L., 2010a. Constraints on average Taiwan reference Moho discontinuity model – receiver function analysis using BATS data. Geophys. J. Int. 183, 1–19.
Wang, H.L., Zhu, L., Chen, H.W., 2010b. Moho depth variation in Taiwan from teleseismic receiver functions. J. Asian Earth Sci. 37, 286–291.
Wang, Z., Fukao, Y., Zhao, D., Kodaira, S., Mishra, O.P., Yamada, A., 2009. Structural heterogeneities in the crust and upper mantle beneath Taiwan. Tectonophysics 476, 460–477.
Webb, S.C., 2007. The Earth's 'hum' is driven by ocean waves over the continental shelves. Nature 445, 754–756.
Wu, F.T., 1978. Recent testonics of Taiwan. J. Phys. Earth 26, S265–S299.
Wu, F.T., Rau, R.J., Salzberg, D., 1997. Taiwan orogeny: thin-shinned or lithospheric collision. Tectonophysics 274, 191–200.
Wu, Y.M., Chang, C.H., Zhao, L., Shyu, J.B.H., Chen, Y.G., Sieh, K., Avouac, J.P., 2007. Seismic tomography of Taiwan: improved constraints from a dense network of strong motion stations. J. Geophys. Res. 112, B08312.
Yang, Y., Ritzwoller, M.H., 2008a. Characteristics of ambient seismic noise as a source for surface wave tomography. Geochem. Geophys. Geosyst. 9, Q02008.
Yang, Y., Ritzwoller, M.H., 2008b. Teleseismic surface wave tomography in the western US using the Transportable Array component of US Array. Geophys. Res. Lett. 35, L04308.
Yang, Y., Li, A., Ritzwoller, M.H., 2008a. Crustal and uppermost mantle structure in southern Africa revealed from ambient noise and teleseismic tomography. Geophys. J. Int. 174, 235–248.
Yang, Y., Ritzwoller, M.H., Levshin, A.L., Shapiro, N.M., 2007. Ambient noise Rayleigh wave tomography across Europe. Geophys. J. Int. 168, 259–274.
Yang, Y., Ritzwoller, M.H., Lin, F.C., Moschetti, M.P., Shapiro, N.M., 2008b. Structure of the crust and uppermost mantle beneath the western United States revealed by ambient noise and earthquake tomography. J. Geophys. Res. 113, B12310.
Yang, Y., Zheng, Y., Chen, J., Zhou, S., Celyan, S., Sandvol, E., Tilmann, F., Priestley, K., Hearn, T.M., Ni, J.F., Brown, L.D., Ritzwoller, M.H., 2010. Rayleigh wave phase velocity maps of Tibet and the surrounding regions from ambient seismic noise tomography. Geochem. Geophys. Geosyst. 11, Q08010.
Yao, H., van der Hilst, R.D., 2009. Analysis of ambient noise energy distribution and phase velocity bias in ambient noise tomography, with application to SE Tibet. Geophys. J. Int. 179, 1113–1132.
Yao, H., Beghein, C., van der Hilst, R.D., 2008. Surface wave array tomography in SE Tibet from ambient seismic noise and two-station analysis – II. Crustal and upper-mantle structure. Geophys. J. Int. 173, 205–219.
Yao, H., Xu, G., Zhu, L., Xiao, X., 2005. Mantle structure from inter-station Rayleigh wave dispersion and its tectonic implication in western China and neighboring regions. Phys. Earth Planet. Inter. 148, 39–54.
Yao, H., Gouédard, P., Collins, J.A., McGuire, J.J., van der Hilst, R.D., 2011. Structure of young East Pacific Rise lithosphere from ambient noise correlation analysis of fundamental- and higher-mode Scholte-Rayleigh waves. C.R. Geosci. 343, 571–583.
Yao, H., van der Hilst, R.D., Montagner, J.P., 2010. Heterogeneity and anisotropy of the lithosphere of SE Tibet from surface wave array tomography. J. Geophys. Res. 115, B12307.
Yao, H., van der Hilst, R.D., de Hoop, M.V., 2006. Surface-wave array tomography in SE Tibet from ambient seismic noise and two-station analysis – I: Phase velocity maps. Geophys. J. Int. 166, 732–744.

Yao, H., Campman, X., de Hoop, M.V., van der Hilst, R.D., 2009. Estimation of surface wave Green's functions from correlation of direct waves, coda waves, and ambient noise in SE Tibet. Phys. Earth Planet. Inter. 177, 1–11.
Yeh, Y.H., Shih, R.C., Lin, C.H., Liu, C.C., Yen, H.Y., Huang, B.S., Liu, C.S., Chen, P.Z., Huang, C.S., Wu, C.J., Wu, F.T., 1998. Onshore/offshore wide-angle deep seismic profiling in Taiwan. Terr., Atmos. Ocean. Sci. 9, 301–316.
You, S.H., Gung, Y., Chiao, L.Y., Chen, Y.N., Lin, C.H., Liang, W.T., Chen, Y.L., 2010. Multiscale ambient noise tomography of short-period Rayleigh waves across northern Taiwan. Bull. Seismol. Soc. Am. 100, 3165–3173.
Yu, S.B., Chen, H.Y., Kuo, L.C., 1997. Velocity field of GPS stations in the Taiwan area. Tectonophysics 274, 41–59.
Zeng, X., Ni, S., 2010. A persistent localized microseismic source near the Kyushu Island, Japan. Geophys. Res. Lett. 37, L24307.
Zeng, X., Ni, S., 2011. Correction to "A persistent localized microseismic source near the Kyushu Island, Japan". Geophys. Res. Lett. 38, L16320.
Zheng, S., Sun, X., Song, X., Yang, Y., Ritzwoller, M.H., 2008. Surface wave tomography of China from ambient seismic noise correlation. Geochem. Geophys. Geosyst. 9, Q05020.
Zheng, Y., Shen, W., Zhou, L., Yang, Y., Xie, Z., Ritzwoller, M.H., 2011. Crust and uppermost mantle beneath the North China Craton, northeastern China, and the Sea of Japan from ambient noise tomography. J. Geophys. Res. 116, B12312.
Zhou, L., Xie, J., Shen, W., Zheng, Y., Yang, Y., Shi, H., Ritzwoller, M.H., 2012. The structure of the crust and uppermost mantle beneath South China from ambient noise and earthquake tomography. Geophys. J. Int. 189, 1565–1583.